Transactions, SMiRT-23
Manchester, United Kingdom - August 10-14, 2015
Division III, Paper ID 418

Fatigue crack growth and arrest under high-cycle thermal loading using XFEM in presence of weld residual stresses

Said Taheri[1], Van-Xuan Tran[2], Emricka Julan[3] and Nicolas Robert[4]

[1] IMSIA Research Centre, EDF- Lab Clamart France
[2] Modelling and Simulation Centre, EDF Energy R&D, UK Centre
[3] AMA Department, EDF-Lab Clamart France
[4] EDF-DPN, UNIE, Strategic center, Saint Denis, France

ABSTRACT

Cracks have been observed under thermal fatigue in some components made of stainless steel in PWR nuclear plants. This paper focuses on the effects of weld residual stresses (WRS) on fatigue crack growth, using Paris' law and eXtended Finite Element Method (XFEM). A thin pipe with a wall thickness of about 10 mm is considered. The loading is a combination of mean stress (Sm), WRS and a variable amplitude loading (VA) due to thermal fluctuations. Simulations are performed with software Code_Aster.

Concerning crack growth without WRS, different parametric studies have been carried out. Crack growth rate of fully circumferential cracks subjected to a representative fraction of the VA signal is compared with that for semi-elliptical cracks (c/a = 10 or c/a=2). Moreover two cycle counting methods have been compared, using different applied thermal loading sequences.

Relative to crack growth in presence of WRS: Welding simulation of 14 passes in 2D axisymmetric on a pipe with a chamfer was conducted to determine the WRS which is used as an initial stress field for crack growth studies. Four cracks with an initial length of 0.6 mm positioned at different heights in the pipe at the area of local effect of WRS have been considered.

*The results show that***:** in absence of crack growth threshold, important differences in crack growth rates are detected between cracks beginning propagation under small compressive WRS and the ones beginning under tension WRS. It seems possible to explain why some cracks already stopped at 2 mm depth while the others propagate deeper by using the stress intensity factor associated with (Sm+WRS) for different axial crack positions.

INTRODUCTION

Thermal crazing (shallow and dense crack networks) has been discovered in different areas of some old RHR systems in nuclear power plants **figure 1 [1,2]**. Moreover there are several isolated cracks starting from zones with stress singularities: welding toe, surface slope change etc **figure 2 [1].** This crack nucleation has been attributed to thermal fluctuations in the mixing zones **(figure 3).** All RHR systems have been changed in French power plants by eliminating stress concentration zones as weld toes and improving the inner surface, e.g. by polishing. Research works have been undertaken to study the conditions of nucleation and crack arrest in high cycle thermal fatigue in RHR systems. The principal aim of this paper is to determine the influence of weld residual stresses (WRS) on crack growth rate and crack arrest.

Expertises of different areas of old RHR systems of 900, 1300 and 1450MW plants show **[1]** :

- Maximum crack depth about 2.5 mm for all crack networks in principal area of 1300-1450 MW plants **(figure 4)**.

- Maximum crack depth about 2mm for all cracks (network or isolated cracks) for 900 MW plants

It is concluded in **[3]** that the existence of dense and shallow crack networks in high cycle thermal fatigue is due to crack arrest. The arrest is proved by the following logical arguments : the depths of the deepest cracks in networks are identical as those observed in **figure 4** (other results are given **in [4]).** As fatigue crack nucleation in high cycle fatigue is not simultaneous at different coordinates (dispersion on fatigue curve related to surface finish), the identical depth of deepest cracks of a network shows their arrest.
This proves moreover that:

- there is no shielding effect between the two cracks of the same length in a network **[3],**
- thermal transient not enough important to affect crack depth in the mixing zone.

As the deepest cracks of a network are at arrest, coalescence may not be possible. The presence of network becomes a safety factor (in the absence of corrosion), since cracks are created and then stop propagation.

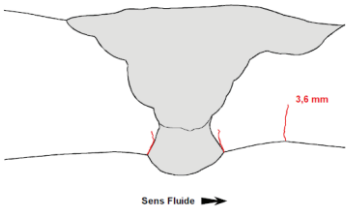

Figure 2 isolated crack nucleated at surface slop change

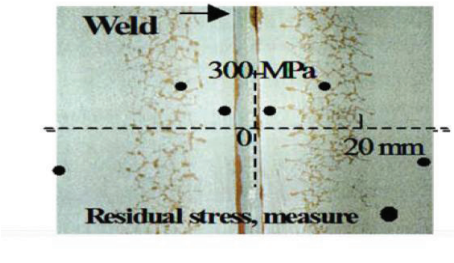

Fig 1 thermal crazing in a RHR system near to a longitudinal weld

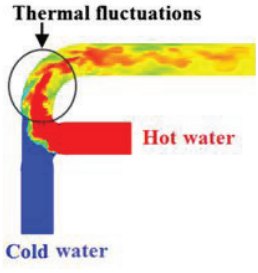

Figure 3 thermal fluctuation on a Tee

While deepest cracks in networks are at arrest near the inner surface of the pipe without any shielding effect, isolated cracks **(figure 2)** usually go a bit deeper **[1].** It's worth noting that the existence of isolated cracks is supposed to be due to the premature crack nucleation at geometrical singularities which shield the creation of new cracks. In absence of shielding effect on deepest cracks of a network these cracks act as singular cracks.

The main issue for a better understanding of thermal fatigue in RHR systems is so to understand why deepest cracks of a network have the same small depth in principal areas of RHR systems, and why isolated cracks nucleated at singular points are deeper than the deepest cracks of networks. One of the aims of this work has been to know if WRS effects may explain these questions.

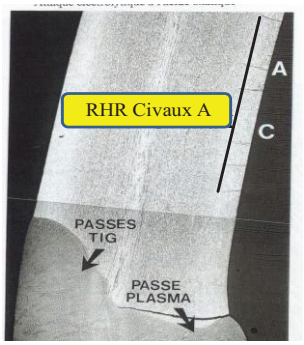

Figure. 4 equal depths for deepest cracks in a network

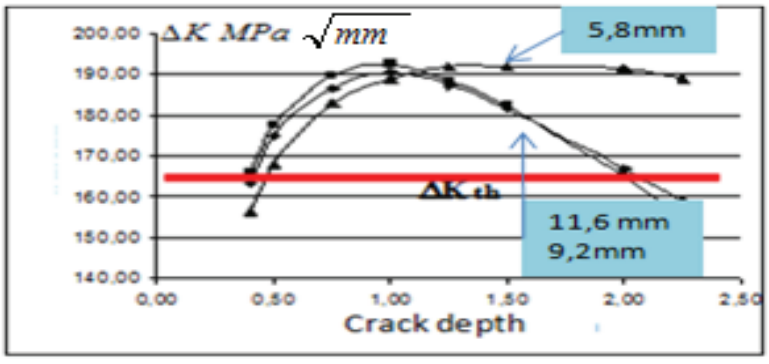

Figure 5 Influence of the thickness of a straight pipe on crack arrest, $\Delta T = 100\,°C$.

CRACK ARREST DUE TO FATIGUE CRACK GROWTH THRESHOLD (FCGT)

Under thermal constant amplitude loading, the crack growth may stop if ΔK decreases and falls below the FCGT around 3-5 MPa for long cracks and for 304 stainless steels. The decrease of ΔK is due to the high frequency of thermal loading **[3]. Figure 5** shows that for a tube under sinusoidal thermal loading on internal surface, with an amplitude of 100 °C (uniform along the tube with boundary condition of zero flux on external face) and a frequency of one Hz, there is possibility of crack arrest. The value of 2 mm at arrest is quiet the same as one given in expertise of RHR systems. Moreover it may be noted an inverse relation between crack depth and pipe thickness.

WRS : STANDARD & TAPERED (WELD) AREA VERSUS LOCAL & STRUCTURE EFFECT

Engineering design separates a straight pipe with a circumferential weld into two parts: Tapered (weld) area and the complement part which is designed by standard area. Tapered area is usually considered to have a detrimental effect on fatigue life by presence of geometrically singularities but also thickness reduction. The effect of WRS on crack nucleation in old RHR systems has been analyzed in **[2].** Absence andpresence of cracks in some areas may be related to WRS. This analysis is based on numerical simulation of WRS. The welding simulation is a difficult task in terms of validation of the simulation. So we used results of a simulation carried out under common work between CEA-EDF-AREVA and validated experimentally **[5].** This is the axisymmetric numerical simulation of 13 passes on a straight thin pipe with a chamfer (pipe thickness $h = 12.8\ mm$ is almost the thickness of principal pipe of a 900 Mw RHR system). **Figure 6 [2]** shows that at internal surface axial and circumferential WRS may be decomposed into 2 parts: a local 3D effect (in tension on inner surface of the tube) on a length of the order of $2*h$ (h is the thickness of the pipe) from the weld and a structure effect (in compression on the inner surface of the tube) given by the theory of thin shell with a characteristic length ($\sqrt{h*r_m}$). It must be noted that WRS local effect area is almost superposed to tapered area which may create confusions between different phenomena. As may be noted on the **figure 6** on the area of structure effect under compression there is no crack. Close to the weld presence of uni-directional axial cracks (out of weld toe) may be related to the largest WRS component which is a circumferential stress. In standard zone where the effect of WRS disappears a multi-directional crack network is observed.

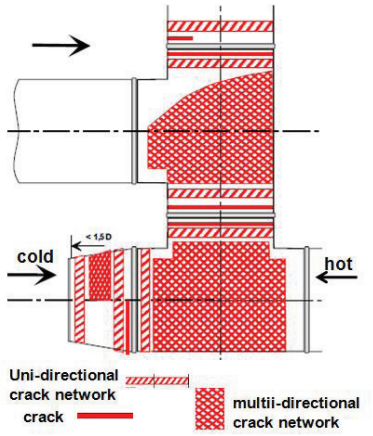

Figure 7 Uni-directional crack network versus local effect of WRS

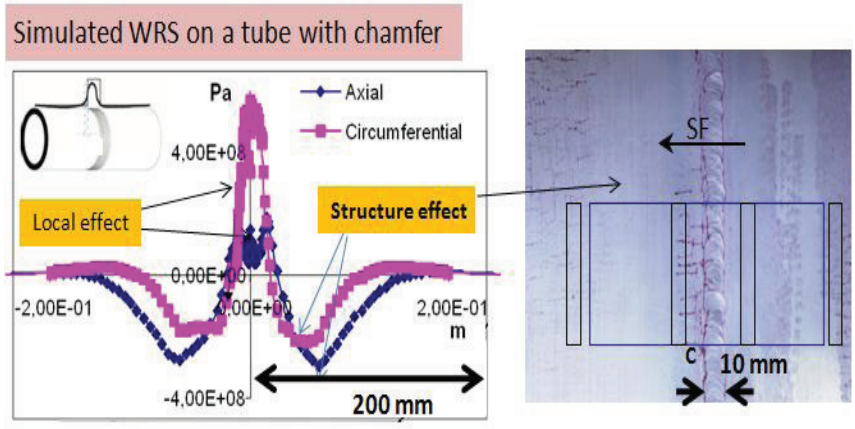

Figure 6 Calculated stress fields on a tube with a chamfer obtained by numerical simulation of WRS (left) and crack network configurations of the straight pipe of a RHR system (right)

Schematic **figure 7 [1]** based on data of thermal fatigue crazing in old RHR systems of French power plants shows as in **figure 6,** starting from the weld, existence of uni-directional crack network near the weld, a non-cracked area, and then a multi-directional cracked area. On many other old RHR systems we observe the same situation. Explanation of uni-directional crack network in region of weld local effect may be given through values of axial and circumferential stresses: nucleation is enhanced perpendicular to the direction where WRS is the largest. Due to the retard in nucleation in other direction, the crack may become enough large to shield nucleation for the other direction. However the question may be raised: why as the thermal loading is isotropic (this is different from a thermal transient which has a direction) a combination of two component of WRS does not determine a crack direction which would be neither axial nor circumferential. The work in **[6]** on crack nucleation under biaxial mean stress and thermal loading shows that only the largest value of mean stress has an impact on critical plane. However the situation is different when both components are identical because thermal loading is isotropic. This may be the case of axial weld in **figure** 1, where cracks have not directions parallels to axial or circumferential directions but are nearly at 45°.

Crack propagation under WRS

The simulation of 13 passes does not fill in totally the chamfer, a 14th pass has then been simulated to completely fill in the chamfer as we have to analyze crack propagation in depth. **Figure 8** shows the axial stress field obtained, which impacts circumferential crack growth in mode I. The problem is symmetrical with respect to the plane of the middle of the pipe. We are only interested in area 0 <Y <26. In fact, 26 mm is twice the thickness (2*12.8), and the previous area is the one of WRS local effect which is mostly in tension. It is in these areas of principal zones of old RHR systems that isolated cracks which are deeper than the deepest crack in the networks are present. So only crack propagation on this area is considered. Axial stress fields at different heights are plotted against depth in **figure 9**.

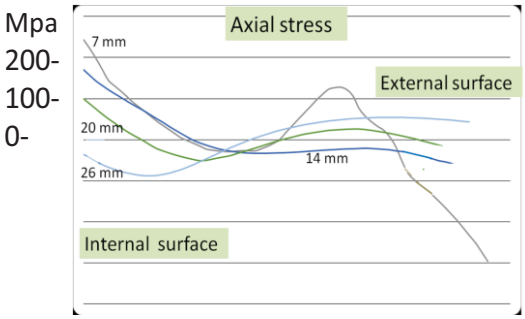

Figure 9 axial WRS versus depth at different heights

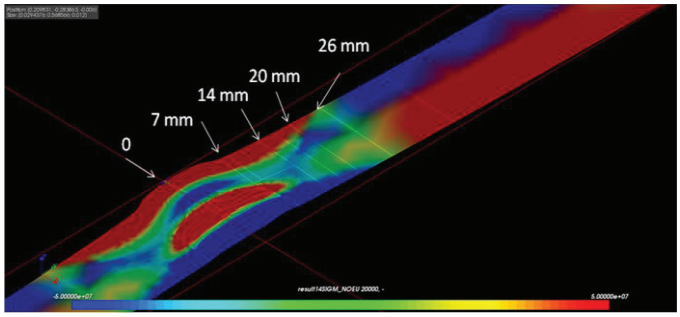

Figure 8 Axial WRS after 14 passes of welding representation between +/-50 MPa (red tension, blue compression)

PARIS' LAW, COUNTING METHOD, AND CODIFIED MODELING OF PROPAGATION

In this study, we are interested only in mode I propagation. In RSE_M code **[7]** the effect of mean stress has been taken into account through the formula (1), where ΔK is the variation of stress intensity factor (SIF) under elasticity hypothesis. No plastic correction under thermal loading is applied. For austenitic stainless steels the conservative value of Paris parameter is $C = 1.8 * 10^{-9}$ for PWR environnement. da/dn is given in mm/cycle et ΔK in MPam$^{1/2}$.

$$\frac{da}{dN} = C\left[\frac{\Delta K}{1 - R/2}\right]^4 \text{ where } R = K_{\min}/K_{\max} \qquad (1)$$

Mean stress (σ_m) effect in this paper is taken into account only on crack opening. So in absence of Fatigue crack growth threshold (FCGT) Paris' law is used in this paper as :

$$da/dn = C(\Delta K_{eff})^m \qquad \text{where} \quad \Delta K_{eff} = K_{\max} - K_{op} \qquad (2)$$

Where K_{op} is the value of SIF for which the crack opens. For $R = 0$ this modelling gives the same fatigue crack growth rate (FCGR) as RSE_M code. Otherwise for $R > 0$ this modelling is less conservative than RSE_M. For all simulations we take $K_{\min} = 0$ when $K_{\min} < 0$ (closed crack). Moreover if two mean tensile stresses fully open a crack under identical load variation, they produce the same crack growth rate. A Paris law with FCGT is also used in this paper (formula 3) with the same mean stress effect :

$$da/dn = C(\Delta K_{eff} - \Delta K_{th})^m \qquad \text{where} \quad \Delta K_{eff} = K_{\max} - K_{op} \qquad (3)$$

Identification of Paris law for a EDF-304-CLI stainless steel with and without threshold : Furthermore we identified the Paris law from experimental data; da/dn versus ΔK given in **[8]** for R=0.7. The results of identification with and without threshold are given in Table 1. Two identifications without threshold are made. As experimental curve shows a shift at a value about $\Delta K = 10\ MPa\sqrt{m}$. For $R = 0$, RSE_M law with $C = 1.8*10^{-9}$ and the law with $C = 9*E-9$, $m = 3{,}13$ give identical crack growth rate **[4]** for $\Delta K = 10\ MPa\sqrt{m}$, while under this value previous identified law is more conservative than RSE_M but not very different.

	Without threshold-1	Without threshold-2	With threshold
C	9.10^{-9}	3.10^{-9}	$1.06*10^{-7}$ 1
m	3.13	3.13	2.43
$\Delta K_{threshold}$			3.34

Table (7.1) Identification of Paris law for a 304 steel grade CLI at R=0.7

Variable amplitude loading in Paris law and the counting method : The counting method is usually *Rainflow* counting which is applied to SIF versus time. 3 methods have been used in this paper**:**

- Paris_FCGT : introduction of a FCGT in Paris law
- Paris_QCM : SIF amplitudes smaller than crack growth threshold are neglected in the counting method as in codified method, while R is taken into account in less conservative way we call "Quasi Codified Method"
- Paris_Total : no amplitude is neglected and a Paris law without threshold is used

CRACK GROWTH SIMULATION IN ABSENCE OF WRS UNDER VARIABLE AMPLITUDE LAODING

Thermo-hydraulic simulations on an RHR mixing tee are not yet sufficiently improved. Simulations for engineering applications are carried out on the main tube of a RHR system or a Mock-up of a RHR system. The Mock-up considered for these simulations is named Father which is a mock-up of a 1300 MW RHR system mixing tee **[9].** The thermal variable amplitude loading used for simulations is the signal F111113N (**figure 10**) issued from the mock-up Father.

Numerical simulations of propagation of fully circumferential cracks and initially semi-elliptical circumferential cracks with XFEM method are carried out with software Code_Aster [**10**]. X-FEM's major advantage is that it represents the crack without explicitly meshing it. So, different crack propagation steps can be performed on initial mesh without cracks **(figure 11])**. Moreover for XFEM method unlike remeshing, crack frontier may get any free form, while for remeshing it must stay semi-elliptical. Results obtained with XFEM have been validated using remeshing **[11]**.

The purpose of this section is to evaluate the importance of different parameters on crack growth rate by FE simulations on geometry of principal pipe of Father mock-up, and to compare the results of crack growth obtained numerically with the experimental results in Father's test. A numerical simulation of crack growth with the previous signal requests a considerable CPU time, thus a part of the signal is selected and is repeated.

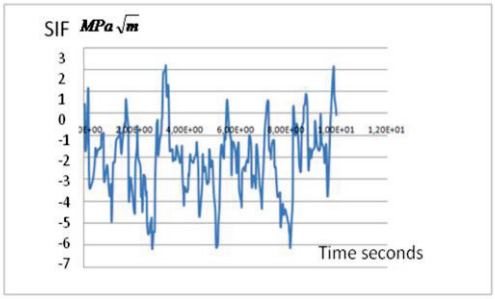

Figure 10 SIF due to FATHER thermal signal on 10 seconds for a crack of 0.6 mm depth

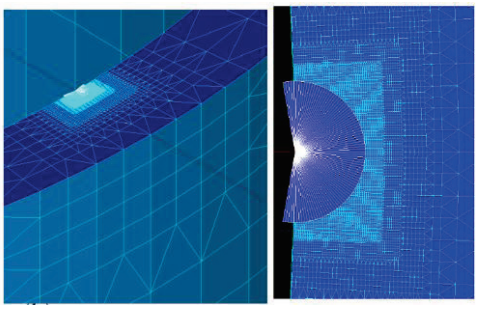

Figure 11 XFEM mesh for a semi-elliptical circumferential crack

Simulation data

Geometry of the structure: The principal pipe of The FATHER mock-up is modelled by a straight pipe sufficiently long and the thickness, e = 7.5mm, and mean radius (R = 75 mm).
Crack geometry: circumferential cracks, and initially semi elliptical circumferential cracks with c/a = 2 (non-elongated crack) and c/a = 10 (elongated crack) are used. Aspect ratio may reach the value of c/a = 20 for some cracks in RHR systems.
The initial crack depth: the initial crack depth is chosen equal to 0.6 mm. For a 304 stainless steel longue cracks have a length higher than a value between 0.5 and 0.8 mm. In our simulation an initial crack length of 0.6 mm is so chosen.
Variable thermal loadings: sequences with different duration have been extracted from Father signal.
Constant permanent mean loading (σ_m): Different values are taken: 0, 20, 50, and 100 MPa etc.

Comparison between different Paris type laws without FCGT

In this paper, both Paris_Total and Paris_FCGT are used. Simulations show (**Table 1)** that for the Father signal negligible difference exists between results obtained by Paris_Total, and Paris_QCM. We may so suppose that they give the same results. Moreover for $R = 0$ Paris_QCM is identical to RSE_M. and for $R > 0$ Paris_QCM is less conservative than RSE_M. As a consequence we may suppose that Paris_Total is less conservative than RSE_M for father loading. Moreover the condition $R > 0$ is an acceptable hypothesis as we will see later for $\sigma_m = 50\ MPa$ cracks are fully open on a cycle.

	Paris-Tot	nearly CODIFIED	% of cycles 69% for $\Delta K < \Delta K_{th}$	Paris-Tot	nearly CODIFIED	% of cycles 75% for $\Delta K < \Delta K_{th}$
Δa mm for 1 bloc	6,53E-06	5,68E-06	$\Delta K_{\max} = 5.84\ MPa\sqrt{m}$	1,05E-5	8,51E-06	$\Delta K_{\max} = 6.16\ MPa\sqrt{m}$
Bloc number	15312	17605		9451	11749	
Hours for 0.1 mm	42,53	48,90	Difference 13%	52,50	65,27	Difference 20%

Table 1 : Comparison of time for propagation length of 0.1 mm between, Paris_QCM and Paris_Total: , $m = 3{,}13 \quad C = 3*e-9$) for two different sequence 10 s (left) and 20s (right)

Parametric studies in absence of fatigue crack growth threshold with Father loading.

For following results we used Paris_Total with $C = 9*E-9$, $m = 3{,}13$ and Paris_FCGT

Comparison of rainflow and "sequential" counting show no significant difference between two methods **[4].** In the "sequential" counting two half successive un-equal variations of loading are replaced by two other half variations equal to the highest value of un-equal variations.

Representativity of the loading sequence**:** In absence of a threshold for a 2D axi-symmetric crack, 10 seconds of thermal loading could be considered acceptable, (for a crack depth less than 2mm) **figure 12**. The same result is obtained for a 3D crack with c/a=2 **[4].**
Comparison between axisymmetric and 3D solutions: As shown in the **figure 13**, until a crack length of 1,2 mm, there is a quasi superposition of crack depths between axisymmetric and 3D solution for c/a=10, and crack growth rate for a 2D axisymmetric case is conservative compared to the 3D case with c/a=2.

Mean stress effect: on **figure 12** one can see that, for the axi-symmetric solution, CGR are identical for $\sigma_m = 50\ MPa$ and $\sigma_m = 100\ MPa$. This is because the crack is fully open on a cycle under these mean stresses. $\sigma_m = 50\ MPa$ is almost the limit case for which under Father loading crack stay permanently open.

Effect of crack initial length**:** a simplified calculus [**4**] shows that 20% error on initial crack length around 0.6 mm gives 40% error on crack depth after 300 hours (Father test) of propagation.

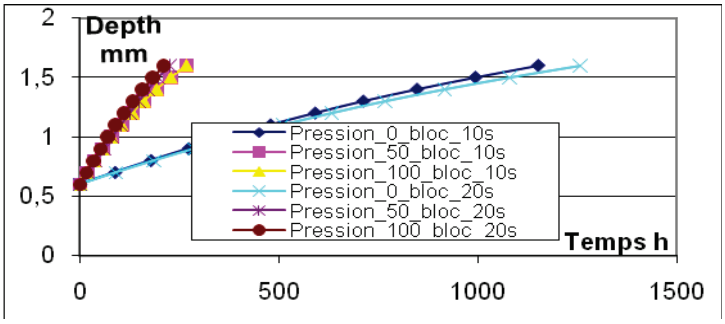

Figure 12 Axisymmetrical simulation: mean stress effect and sequence duration effect

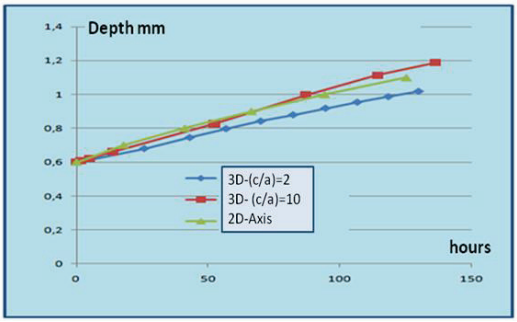

Figure 13 Comparison of different modeling for a sequence of 2s with $\sigma_m = 0$

Parametric studies in presence of FCGT

Representative loading in presence of FCGT is used for an axi-symmetric solution. Taking into account FCGT, it requires at least a sequence of 100 seconds (probably more) to be representative for this type of study (**figure14**). In fact since Father loading has many small amplitude loads, after elimination of small amplitude loading by FCGT there would not exist enough cycles for counting.

Comparison between Father test results and simulation results:

For the Father test the deepest cracks have a depth of 0.9 mm after 300 hours of operation. Without FCGT axisymetrical simulations with a $\sigma_m = 50\ MPa$ gives a crack depth of 1.8 after 300 H. For a semi-elliptical crack (c/a=2) simulation is carried out only with a sequence of 2 seconds (**figure15**) due to CPU time**.** We get 1,4 mm against 0.9 mm. Both results are conservative. Axisymetrical simulation *with* FCGT for a sequence of 100 seconds give a crack depth about 0.9 mm at 300 hours. This would look perfect, however in 300 hours there is a part of nucleation (about 100 hours), a part of short crack growth. Moreover simulation with a sequence larger than 100 seconds has to be performed.

AXI-SYMMETRIC CRACK GROWTH SIMULATION IN PRESENCE OF WRS IN ABSENCE OF FCGT (PIPE THICKNESS 12.8 mm)

The principal aim of this section is to determine the influence of WRS on FCGR. After welding simulation of a straight pipe with a chamfer on an initial mesh, WRS have been transferred to a more refined un-deformed mesh to study circumferential crack propagation. The loading is a combination of a Thermal variable amplitude (VA) load issued from Father mock-up test, axial WRS, a permanent mean stress $\sigma_m = 50$. It is shown that on the un-deformed mesh, the mode I propagation is dominant. Cracks are located at different heights: 7mm, 14 mm, 20 mm, 26 mm in the area of weld local effect. Moreover a linear combination of SIF for the three loadings is verified under elasticity hypothesis in Code_Astre, which permits to analyse the effect of different loadings on crack propagation.

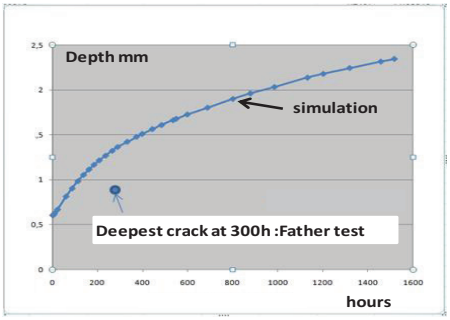

Figure15 3D (c/a=2) crack propagation with a sequence of 2s , $\sigma_m = 50$.

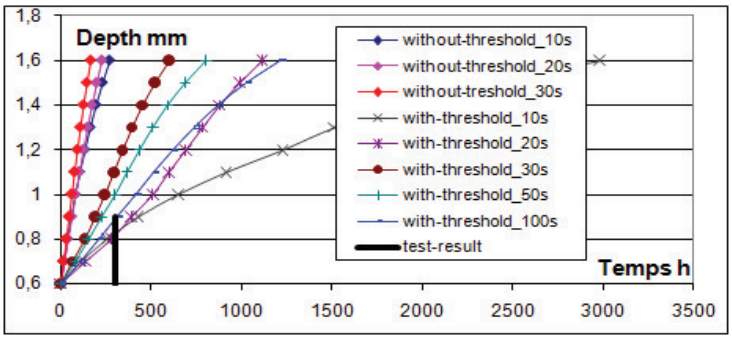

Figure14 Axisymmetric simulations, representivity of load sequence with and without crack growth threshold $\sigma_m = 50$

SIF due to the WRS and the permanent mean stress

SIF due to WRS (axial stress): WRS are self-equilibrated (**figure 9**). Moreover when the crack propagates WRS is modified to take into account this balance. **Figure 16** shows that for heights of 7, 14, 20 mm, cracks start to propagate in an area of tensile WRS. However SIF remains always positive despite of the areas of strong compression (compression before crack starts propagation, e.g. for 7mm height) near the external surface. Moreover For the height of 26 mm, where the crack starts propagation under compression, SIF remains negative, despite the tensile zone (tensile before crack starts propagation) in the depth (**Figure 16**). These results show that it is not possible to analyze the effect of WRS on crack growth through WRS field, but only through SIFs associated with the WRS fields.

SIF associated to the summation $(\sigma_m = 50MPa) + WRS$**: Figures 17** shows respectively SIFs associated with $(\sigma_m = 50MPa) + WRS$. Note that for the height of 26 mm the SIF associated with $(\sigma_m = 50MPa) + WRS$ is almost zero up to 5mm. As indicated by this **figure**, this result is related to an initial crack growth under compressive WRS.

Discussion

For two different mean loads (represented by WRS or by σ_m or by σ_m +WRS) if the crack remains completely open during growth, crack growth rates are identical for both cases if cracks have the same lengths. Moreover the effect of permanent mean stress for crack opening is more and more important as crack length increases. Note that $\sigma_m = 50$ MPa is almost a limit case for which the crack is fully open all the time under Father loading in absence of WRS. For high frequencies (e.g. 1 Hz) after some crack growth (**figure 3**), SIF amplitude due to thermal loading decreases with crack growth. With a power 4 in

Paris3's law, crack growth rate may be up to 16 times greater in presence of a mean stress which opens fully the crack compared to zero mean stress. Crack growth rate is then issued from a competition between the weakening in the depth of the SIF amplitude due to high frequency of thermal loading and more opening of the crack due to the increase of mean SIF with crack length.

Results, crack depth versus time

- **A**: The crack at the height 7 mm (almost in the seam) and the crack at the height 14 mm have the same behavior (**figure 18)** despite different WRS. The reason is that σ_m + WRS keeps the crack fully open in both cases from the length of 0.6 mm.
- **B**: The same arrest depth at about 12.6 mm for three cracks at height 7, 14, 20 mm (near external surface) are obtained **(figure 18).** This may come from a decrease of SIF amplitude for high frequency thermal loading. So, cracks are fully open but the amplitude of the thermal load should be almost zero even for a fully open crack.
- **C**: The crack at the height 20mm has a behavior different from cracks at 7-14 mm. But its arrest depth is the same as for 7 and 14 mm. This comes from the fact that crack at 20 mm height is not fully open between 3mm and 8 mm. After being partially open between 3 and 8 mm the crack at 20 mm becomes fully open like cracks at 7 and 14 mm, and as has been explained before they will have the same arrest depth.
- **D**: The crack at the height 26 mm is almost at arrest at 2mm depth without any FCGT, **figure 19** (in fact crack depth after millions of hours is 4 mm). The reason is that the mean stress is zero at the beginning of crack growth. We can see this in **figure 17** where the SIF of (σ_m +WRS) is almost zero along 5 mm depth. The propagation for the height 26 mm is therefore only with Father loading. This suggests that at 5 mm depth the SIF amplitude due to Father loading becomes almost negligible. The difference between this paragraph (D), and paragraph A is that for A cracks are fully open.

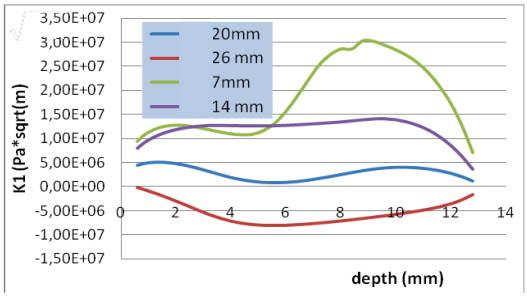

Figure 16 SIF of WRS for cracks at different heights

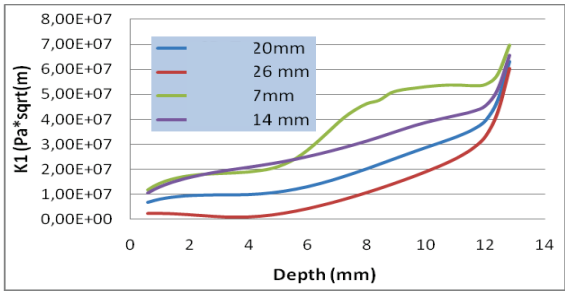

Figure 17 SIF for sum of SIF ($\sigma_m = 50$ MPa+WRS)

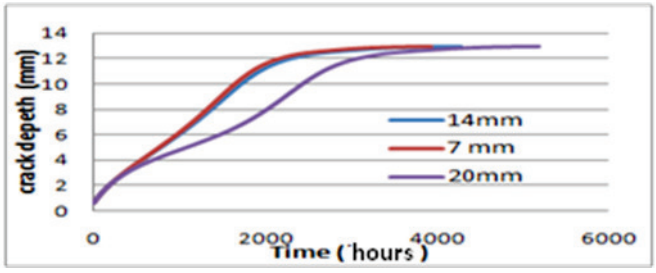

Figure 18 : crack growth rate and arrest close to Outer face , starting under positive WRS

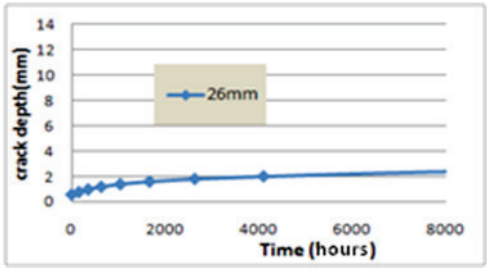

Figure 19 crack starting propagation under compressive WRS is almost at arrest at 2mm

CONCLUSIONS

1-The effect of WRS on crack propagation cannot be determined through analysis of the shape of WRS field in the depth but through associated SIF as WRS relaxes during crack propagation. The accounting of WRS effects in some codifications via a direct summation of WRS in the stress formulas for crack propagation study appears not to be quite always consistent.

2- For a fully circumferential crack on a straight pipe with the same thickness as the principal pipe of a 900 MW RHR system, propagating under Father loading, RSE_M propagation law gives too large and not realistic depth *It is necessary to use a FCGT in the simulation to justify crack depths (at arrest) for the RHR systems.*
Conclusions hereafter are issued from logical argumentation so are independent of Paris's law parameters.

3-Crack is fully open before arrest: This case gives the maximum depth at arrest and explains the identical depth for deepest cracks of a network. This case may occur for both cases of cracks fully or partially open when crack starts propagation. *An important conclusion is that, maximum crack depth at arrest is determined only by ΔK of the thermal loading in presence of FCGT and not by the mean value of SIF***.**

4-Crack is not fully open at its arrest : In this case, contrary to previous conclusion, the crack depth at arrest depends on mean stress (σ_m and WRS, or others). This case is produced for a sufficiently large compressive WRS as σ_m is positive and large enough compared to Father loading.

5-Due to conclusion 1, neither WRS nor any other mean stress is able to explain why some isolated cracks nucleated at singularities have depths larger than the deepest cracks of the network. **The final conclusion concern the safety of the principal area of some RHR system principal pipe, it may be concluded that in absence of geometrical singularities maximal crack depth is the same as the deepest cracks in a network when there exist two cracks with identical depths**.

REFERENCES

[1] Robert, N., (2002) Report EDF/DPN D4009.27.02.REA/RBT.02/0385.
[2] Taheri S. (2007). "Some advances on understanding of high cycle thermal fatigue crazing". ASME J Press Vessel Tec. 129:400–10.
[3] Taheri, S., Sbitti, A., (2010). « Crack arrest in high cycle thermal fatigue". Nuclear Eng Design : vol. 240, n°1, pp. 30-38 :
[4] Taheri S., (2014) "Synthesis of studies on fatigue crack growth and their arrest in RHR systems with XFEM method in presence of weld residual stresses". Report EDF H-B60-2014-11451-EN.
[5] Razakanaivo, A., Desroches, X., Bois, C., Lejail, Y., Kichenin, J. (2000). « Tubular welding numerical simulation: experimental validation", Proc. ICRS-6, 2000.
[6] Lei, B.M, Tran, V.X, • Taheri S., Wan, L., Zhou, Y. (2014) "An analytical study on cracking directions and damage in thermal fatigue crazing subjected to variable amplitude loadings" Mater Sci, 49:5546–5563.
[7] RSE_M : Règles de Surveillance en exploitation des matériels Mécaniques des îlots Nucléaires REP, tome II, édition.
[8] J.C. Le-Roux, M. Akamatsu, report HT-26/02/027/B.
[9] Vincent, L., Chaise, S., Braillard, O., Le-Roux, J.C., Taheri, S., Beaufils. R. (2009). "On the significant difference of lifetime prediction between strain and stress control analysis". Proceeding of 2th Int. conf. on material and component performance under variable amplitude loading. Darmstaat, Germany, 2009:23–26.
[10] http://www.code_aster.org
[11] Julan, E., (2011). Etude de la propagation d'une fissure allongée sous chargement à amplitude variable. Raport CDD Lamsid 1/10/2011.